

# Shock-induced collapse of a cylindrical air cavity in water: a Free-Lagrange simulation

G.J. Ball<sup>1</sup>, B.P. Howell<sup>1</sup>, T.G. Leighton<sup>2</sup>, M.J. Schofield<sup>1</sup>

<sup>1</sup> School of Engineering Sciences, University of Southampton, SO17 1BJ, UK

<sup>2</sup> Institute of Sound and Vibration Research, University of Southampton, SO17 1BJ, UK

Received 14 September 1999 / Accepted 28 June 2000

**Abstract.** A Free-Lagrange CFD code is used to simulate the collapse of a cylindrical air cavity in water by a 1.9 GPa incident shock. The Lagrangian treatment allows the air/water interface to be tracked throughout the interaction. The incident shock is partially transmitted into the cavity, within which it experiences multiple reflections. The upstream cavity wall involutes to form a high-speed jet which, on impact with the far cavity wall, produces an intense blast wave. Heating of the gas within the cavity is highly non-isentropic, and is dominated by shock heating. The predicted final gas temperature is of order 12000 K, although the modelling assumptions used here lead to over-prediction of temperature during the later stages of collapse.

**Key words:** Free-Lagrange method, Bubble collapse, Detonation initiation, Cavitation, Jetting, Shock heating

## 1 Introduction

This paper reports on a simulation of the response of a cylindrical gas cavity to a shock of GPa order. Experimental investigations of the collapses of “gas discs” have been undertaken for well over a decade (Brunton and Camus 1970; Camus 1971). The objective of this paper is a validation test of the simulation, through comparison of its predictions with the results of one such experiment (Bourne and Field 1992). However it is the axisymmetric collapse of an initially spherical bubble, rather than the compression of a gas disc, which is important to most practical applications. Gas discs were studied because of the ability to control the initial conditions (cavity size, number, position, and composition); and because of the relative ease with which observations can be made, particularly through the use of high speed photography (Dear and Field 1988). These are the very features which recommend it as a geometry for a validation test of the simulation, prior to production of an axisymmetric code (currently under development).

Hence this paper records a step in a process designed to simulate bubble dynamics, and not to investigate the application which was the impetus behind the experimen-

tal studies (specifically the role of cavities in the initiation of reaction in commercial explosives). However an appreciation of the considerations given to that role provides a useful perspective on features seen in the simulations presented here. These are, specifically, the compression of gas and the applicability of “adiabatic” approximations (see below) in predicting temperature rise; the involution of cavities to form jets, and the hydrodynamic effects when these subsequently impact the far bubble wall; the evolution of gas shocks and their reflections from the cavity walls.

Reaction initiation in commercial explosives is a thermal effect, and under conditions where bulk heating is insufficient to cause ignition, reaction might be initiated through hot-spots (Bowden and Yoffe 1952, 1958; Heavens and Field 1974; Winter and Field 1975). Adiabatic compression of gas pockets was identified as one amongst a range of mechanisms by which such hot-spots might be produced (Bowden and Yoffe 1952, 1958; Coley and Field 1973; Chaudhri and Field 1974; Starkenberg 1981; Field et al. 1982). Chaudhri et al. (1982) and Chaudhri (1989) observed an initiation which was attributed to the impact of a high speed jet which developed within the collapsing cavity. That jets could form had been suggested by Kornfeld and Suvorov 1944, and observed two decades later (Naudé and Ellis 1961; Walters and Davidson 1962, 1963; Benjamin and Ellis 1966; Lauterborn and Bolle 1975). Since then cavitation jets have been examined extensively. High speed photography has played a key role in under-

---

*Correspondence to:* G.J. Ball (e-mail: gjb1@soton.ac.uk)

An abridged version of this paper was presented at the 22nd Int. Symposium on Shock Waves at London, United Kingdom, from July 18 to 23, 1999

standing and measuring the process (see reviews by Field 1987; Blake and Gibson 1987; Steinberg 1993; Philipp and Lauterborn 1998). Such observations are particularly challenging because of the rapid timescales and small length-scales involved.

The formation of jets during cavity collapse has relevance beyond the issue of the sensitisation of explosives. The impact of jets against solids causes erosion pits (Preece 1979; Preece and Hansson 1981; Tomita and Shima 1986; Lush et al. 1987; Okada and Iwai 1989; Iwai and Okada 1989; Philipp and Lauterborn 1998) and pressure transients (Jones and Edwards 1960; Radek 1972; Hinsch and Brinkmeyer 1976; Ebeling 1978; Blake et al. 1986; Vogel et al. 1989). Although jet-induced solid erosion is often undesirable, it can be exploited in cavitation cleaning (Zequiri et al. 1997) or in extracorporeal shock wave lithotripsy (see review by Takayama 1999).

It is important, at this point, to appreciate the ambiguous way in which the term “adiabatic” has been conventionally used in the cavitation field. Although it (correctly) implies an absence of heat transfer, it has also been applied to models of gas heating by compression in which the gas properties are assumed to be spatially uniform, and to which an isentropic ( $pv^\gamma = \text{constant}$ ) or polytropic ( $pv^n = \text{constant}$ ) law is applied. Thus “adiabatic” has been used in a sense which excludes shock heating, although the character of shock heating is in practice adiabatic. We will continue to use the term in this conventional, but thermodynamically imprecise, sense in this paper. The adiabatic approximation has been used extensively, not just in the study of air discs, but throughout the field of collapse cavitation dynamics to predict the temperature rise in the gas. Indeed, an adiabatic calculation, spatially-averaged over the bubble gas, forms the basis of the “Mechanical Index” (Holland and Apfel 1989; Apfel and Holland 1991), which is used as a real-time display during ultrasonic diagnostic scanning to assess the likelihood of cavitation *in vivo* (AIUM/NEMA 1992).

The present study is particularly concerned with the thermal characteristics of cavities which involute to form jets. Bowden and Yoffe (1958) considered an adiabatic model of the compressed gas to be appropriate, given the speed of compression. Chaudhri and Field (1974) came to the same conclusion by observing the ignition of single crystals of silver or lead azide, or pentaerythritol tetranitrate, to which bubbles had been attached. However, some doubts about the ability of an adiabatically-heated gas to explain ignition in rapid collapses were raised (Starken-berg 1981). Scales in both distance and time are important for heat conduction from the compressed gas to the liquid at the bubble wall (Chaudhri and Field 1974; Starkenberg 1981), or to the small liquid droplets which are spalled off the wall into the gas pocket (Johansson 1958), or to the liquid in the jet. Other possible causes of ignition were identified. Frey (1985) attributed temperature rise to the following sources: heating in the gas phase; hydrodynamic effects (occurring as a result of liquid compressibility during jetting or very rapid spherical collapses); the inviscid plastic work required to overcome the liquid

yield strength; and viscoplastic work. Which dominates may depend on cavity size, liquid viscosity etc. (Mader et al. 1967; Chaudhri and Field 1974; Mader and Kershner 1985, 1989). The numerical simulation presented here incorporates compressive heating in both phases, including non-isentropic compression by shock waves and the effects of liquid jetting. Viscosity and heat transfer have been neglected – these approximations will be justified in Sect. 3.

The experimental scenario against which this simulation is compared involves the two-dimensional collapses of cavities shaped in gel, first developed by Dear and Field (1988). Bourne and Field (1991, 1992) present results from the collapse of large (i.e. mm-order) air discs in a low-viscosity emulsion under high amplitude (GPa) shocks, and conclude that the two main causes of ignition are hydrodynamic heating in the region impacted by the jet, and adiabatic heating of the gas. When collapses occurred in a reactive emulsion, ignition occurred “firstly within the vapour contained within the cavity at the final moments of collapse, secondly in the material adjacent to the heated gas at the downstream cavity wall and thirdly, and principally, by hydrodynamic heating of material at the point of impact of the high-speed jet.” Bourne and Field observed luminescence from the jet impact point and from the gas in the lobes generated as the jet bisects the air disc. The latter had been observed previously by Dear et al. (1998).

Key features, therefore, are the nature of the jet and its impact; and whether the adiabatic approximation is sufficient to estimate the gas temperatures achieved.

In the present work we have produced a numerical simulation of an experimental configuration used by Bourne and Field (1992) – a 6 mm cylindrical air cavity in gelatine/water impacted by a 1.9 GPa shock – in order to gain further insight into the detailed mechanism of the shock/cavity interaction. The study of Bourne and Field (1992) is chosen because of the readiness with which quantified parameters from their data can be tested against the output of the simulation.

The gelatine content in the experiments was 12% by weight, giving a gel density of  $970 \pm 50 \text{ kg/m}^3$ . Bourne and Field state that the gelatine lost its viscoelastic properties when shocked. In this simulation the gelatine/water mixture has been approximated as pure water.

A similar problem was tackled by Lesser and Finnström (1987) using an approximate method. The liquid motion was first calculated using linearised equations, neglecting the influence of the gas. The wave system within the cavity was then predicted using Whitham’s Geometric Shock Dynamics. Their results show some qualitative agreement with the Bourne and Field experiments, and with the early stages of our simulation, but predict only modest gas heating. Critically, their calculations were not continued beyond the first reflection of the air shock from the cavity wall: as will be shown in Sect. 6, our simulation predicts that most of the gas heating occurs after this time.

## 2 Numerical method

The simulation is performed using a recently developed Free-Lagrange CFD code *Vucalm* (Ball 1996), which solves the two-dimensional unsteady Euler equations on an unstructured Lagrangian grid using a Godunov-type method.

The working fluid is divided into discrete packets, between which mass exchange is forbidden; mass conservation errors are therefore entirely avoided. Flow variables are stored at a central “particle” within each packet which convects at the mass-mean velocity of the packet. The approximate locations of the packet boundaries are determined by constructing a Voronoi mesh, in which each particle is enclosed within a polygonal cell. The cells form the control volumes for the time integration of the Euler equations. By definition, in a Voronoi mesh each cell encloses all points in the domain which are closer to the corresponding particle than to any other particle. The mesh is fully reconstructed after every five time steps to allow the grid connectivity to change naturally under the influence of shear. During intervening time steps the mesh vertices are convected at the local flow velocity – algebraic details are given in Ball (1996). The need for frequent mesh reconstruction involves a penalty in computing cost – we estimate that timesteps on which reconstruction is performed require about twice the CPU time of steps on which a pre-existing mesh is convected. For the cavity collapse problem reported here, the total CPU time used was about 280 minutes per microsecond of simulation, on a Pentium II processor.

The use of a conventional conservative computational scheme on an Eulerian mesh will typically produce pressure errors at material interfaces due to the numerical diffusion of the associated density and total energy discontinuities (see, for example, Quirk and Karni 1994). The Free-Lagrange methodology used here avoids this source of error entirely since numerical smearing of material interfaces does not occur. The treatment of multi-material problems is greatly simplified in that the type of fluid in each packet is assigned from the start of the simulation; the fluid type in a given packet never changes, and there are no mixed packets. Hence material interfaces always coincide with mesh cell boundaries, and are sharply resolved; interface tracking or reconstruction algorithms are not required. However, an undesirable consequence is that material interfaces exhibit small-amplitude irregularities on the scale of the mesh cell size, which can trigger Richtmyer-Meshkov instability when strongly shocked. This problem is prevented in the present work by applying a simple interface smoothing routine which acts as a form of artificial surface tension – details will be reported elsewhere (Howell and Ball 1999).

An additional consideration when using a Lagrangian mesh with an explicit scheme is that of timestep management. The maximum stable timestep for the method is limited by the usual CFL criterion. In flow regions subject to large compressions, such as the interior of the air cavity, the mesh itself becomes highly compacted, resulting in an uneconomically small maximum timestep. This problem is overcome in *Vucalm* using a “derefinement” algorithm.

When the timestep falls below a user-specified minimum value, this routine automatically identifies and merges adjacent pairs of fluid packets in regions of excessive mesh density. Merging is strictly conservative, and is only permitted between packets of the same fluid type.

Movement of fluid across freeflow domain boundaries is automatically accommodated. When inflow occurs, fluid packets adjacent to the boundary are allowed to increase in mass at a rate matching the boundary mass flux. When the packet mass has increased by 70% the packet is subdivided into mother and daughter packets and the process is started afresh. When outflow occurs, packets are deleted from the calculation as the corresponding particle crosses the domain boundary.

Three types of Riemann solver are used in this problem. At air/air cell interfaces a version of the HLLC approximate solver (Toro et al. 1994) is used which has been adapted for the Lagrangian frame (Ball 1996). At air/water interfaces an exact solver is employed (Flores and Holt 1981). Finally, at water/water interfaces a “two-shock” variant of the Flores and Holt solver is used – this was found to be more numerically robust than the exact solver, which occasionally failed to converge in the highly sheared flow encountered after jet impact. The two-shock approximation involves the assumption that all local Riemann problems comprise two shocks plus a contact surface – see Toro (1997) for a general discussion of this method.

Each of the above Riemann solvers incorporates an explicit representation of the contact surface in the local Riemann problem. When implemented in the Lagrangian frame, where the cell boundary and the contact surface are coincident by definition, they give zero numerical diffusion at contact discontinuities, and for convecting flow structure in general.

A piecewise-linear reconstruction of primitive variables (density, pressure, velocity) within grid cells is used to obtain nominal 2nd-order spatial accuracy (Ball and East 1999). Time integration is 1st-order – previous experiments with 2nd-order time integration for this scheme have produced negligible improvements in solution quality. A slope limiter, based on the MUSCL approach (Van Leer 1979), is used to prevent the creation of extrema in the local reconstruction, and hence avoid numerical oscillations at shocks. This limiter has been carefully optimised to minimise mesh-induced directional bias – see Ball (1996).

The *Vucalm* code has been used to simulate blast refraction at contact surfaces between dissimilar gases (Ball and East 1996) and at air/foam interfaces (Ball and East 1999).

## 3 Fluid modelling approximations

In order to minimise computational cost and coding complexity, relatively simple models have been used for both water and air behaviour. The modelling assumptions, and their attendant errors, are discussed in this section.

The equation of state for water is here approximated using the Tait equation:

$$p = B \left[ \left( \frac{\rho}{\rho_R} \right)^\gamma - 1 \right], \quad (1)$$

where  $p$  is pressure,  $\rho_R = 999.96 \text{ kg/m}^3$  is a reference density at which the pressure falls to zero, and  $B$  and  $\gamma$  are constants taking the values  $3.31 \times 10^8 \text{ Pa}$  and 7 respectively. Haas and Sturtevant (1987) argues that errors incurred by the use of the Tait equation become significant only when the liquid pressure exceeds 10 GPa. In the present work, the highest predicted pressure is approximately 5 GPa, which occurs briefly during the impact of the liquid jet on the bubble wall; the highest sustained pressure is the incident shock pressure of 1.9 GPa. We therefore conclude that the Tait equation is adequate for our purpose.

The perfect gas equation of state is used in the air bubble for computational convenience. The magnitude of the errors incurred as a result of this choice can be estimated by comparing typical air temperatures from the simulation with values calculated using the Van der Waals equation, for the same pressure and density. At the time of liquid jet impact, the maximum pressure and temperature in the air cavity are approximately 35 MPa and 6000 K. At this condition, the perfect gas equation over-predicts the temperature by 150 K, or +2.6%. At the end of the simulation, the most extreme air state predicted is 300 MPa and 12000 K – in this case the error arising from the use of the perfect gas equation is 1400 K, or +13%. This source of error is therefore only really significant after jet impact, and never grows large enough to undermine the physical basis of the simulation.

Dissociation of air has not been included. Taking the peak gas condition at jet impact (35 MPa and 6000 K), at equilibrium one would expect negligible nitrogen dissociation, and approximately 22% oxygen dissociation, giving a compressibility factor of 1.05. The impact of dissociation is therefore expected to be modest. At later times the degree of dissociation is expected to increase, but the shortage of equilibrium constant data above 6000 K makes this effect difficult to quantify.

Perhaps the greatest source of modelling error arises from the treatment of specific heats, which are assumed to remain constant at their room-temperature values. In reality, due to the increasing excitation of molecular vibrational modes, the equilibrium specific heats for air will increase substantially during the bubble collapse, while the specific heat ratio will fall. During the early stages of collapse, the characteristic time for vibrational relaxation for nitrogen will be comparable to the timescale of the collapse ( $\tau_{\text{vib}} \simeq 1.2 \mu\text{s}$  for 4 MPa and 2800 K), so that vibrational equilibrium will not be achieved, and the effective specific heats will be lower than the equilibrium values. By the time of the jet impact,  $\tau_{\text{vib}} \simeq 0.02 \mu\text{s}$  in the hottest region, so that rapid vibrational relaxation to equilibrium is expected. However, it should be remembered that the peak temperatures behind strong shocks within the bubble will be substantially higher than the equilibrium value, for a period after shock passage of order  $\tau_{\text{vib}}$ , and that these peak temperatures may be of physical importance in processes such as sonoluminescence. The task of simu-

lating the effects of variable specific heats with finite-rate vibrational relaxation was considered too complex for the present study, but is clearly a topic which will require further attention in future work.

Heat transfer has been neglected. The errors resulting from this simplification are difficult to quantify because of the complexity of the flow field and the very significant spatial variation in temperature within the cavity. However, heat transfer is expected to be of less importance than in most cavitation studies because (i) the cavity is relatively large (diameter 6 mm) and (ii) the strong incident shock produces a very rapid collapse ( $\sim 3 \mu\text{s}$ ). An impression of the significance of heat transfer in this problem can be obtained by considering an idealised one-dimensional representation of the heat loss to the water by conduction at the cavity boundary. In this 1D problem, a body of stationary air at uniform initial temperature  $T_0$  is brought into contact with an isothermal heat sink at  $T_s$ . An estimate of the thermal diffusivity  $\alpha$  of the air under representative conditions is required. The effect on thermal diffusivity of increasing temperature and pressure tend to counterbalance, with the result that the value at 4 MPa and 2800 K is  $\simeq 2.0 \times 10^{-5} \text{ m}^2/\text{s}$ , which is close to the ISA sea level value. Using this value of  $\alpha$ , it can be shown that the thermal boundary layer in the air, as characterised by the temperature contour  $T = T_s + 0.9(T_0 - T_s)$ , is only  $\simeq 0.02 \text{ mm}$  thick after  $3 \mu\text{s}$ . Since this is only a very small fraction of the cavity diameter, even during the late stages of collapse, it is concluded that heat transfer is unlikely to be important in this problem.

Finally, the simulation is inviscid, and no account is taken of inter-phase mass transfer or surface tension (but see the discussion on interface smoothing in Sect. 2). In view of the relatively large cavity size, and the dominant influence of water inertia on the flow dynamics, it seems unlikely that viscosity or surface tension will play a major role, while cavity size coupled with the short time scale suggest that inter-phase mass transfer will be unimportant.

To summarise, most approximations, with the probable exception of the use of constant specific heats, will have only modest impact on the simulation. However, the various sources of error in the prediction of temperature all tend to lead to over-estimates, and these errors will become more severe as the collapse proceeds. It is our view that the temperatures predicted for the later stages of collapse (particularly after the liquid jet impact) should be regarded as only semi-quantitative. However, as the flow appears to be dominated by inertial effects in the water, it is considered unlikely that such errors will impact upon the physical character of the collapse.

## 4 Test of numerical accuracy

Previously, the Vucalm code has been successfully validated for a shock tube flow containing a perfect gas – see Ball (1996). In the present context, it was considered desirable to evaluate the numerical accuracy of the code when simulating the interaction of a strong shock with

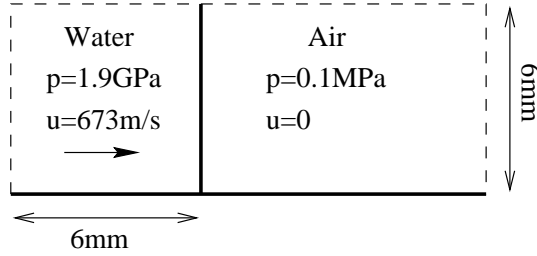


**Fig. 1.** Configuration of the numerical accuracy test problem

a water/air interface, since such events are central to the shock/bubble interaction. The case selected comprises the normal impact of a planar 1.9 GPa water shock onto a planar water/air interface, and represents a one-dimensional equivalent of the shock/bubble problem to be defined in Sect. 5. The test configuration is shown in Fig. 1. A planar water/air interface is positioned at  $x = 6$  mm. At initialisation, the region to the right of the interface contains air at ISA sea level conditions (101325 Pa and 288.15 K). The left hand region contains water which has been processed by a right-running shock, with a post-shock pressure of 1.9 GPa. Thus  $t = 0$  corresponds to the moment of impact of the shock on the interface. The domain geometry and cell mesh density are the same as that used for the shock/bubble problem.

Using the Tait equation of state (Sect. 2), the post-shock water density is  $1313.2 \text{ kg/m}^3$ . Following Flores and Holt (1981), the water velocity is found from

$$u_2 - u_1 = \sqrt{\frac{\rho_2 - \rho_1}{\rho_2 \rho_1} (p_2 - p_1)} \quad , \quad (2)$$

where subscripts 1,2 represent pre- and post-shock conditions respectively. Taking pre-shock conditions as quiescent ISA sea-level yields  $u_2 = 673.19 \text{ m/s}$ .

After initialisation, a strong left-running expansion wave propagates from the interface into the water, while a relatively weak shock is transmitted into the air. The corresponding wave strengths can be found analytically, to any desired accuracy, via an iterative solution of the Riemann problem at the interface – see Flores and Holt (1981) for details. Using this method, the pressure and fluid velocity in the region between the expansion and transmitted shock are found to be  $p_* = 2.7495 \text{ MPa}$  and  $u_* = 1313.4 \text{ m/s}$  respectively. Using standard normal shock relationships for the transmitted air-shock yields a shock Mach number  $M_s = 4.838$ , and a post-shock air temperature  $T_* = 1581.7 \text{ K}$ .

The test problem was run for  $1.5 \mu\text{s}$ , then data was sampled along the domain centreline within the wave-processed regions of both air and water. Seven equi-spaced samples were taken in each region. This data, and its comparison with the analytical solution, is summarised in Table 1. The numerical results are seen to agree very well with theory. In general, the largest errors were found for particles in contact with the water/air interface, but no individual particle property deviated from the analytical value by more than 3%. The relatively large errors asso-

**Table 1.** Results of numerical accuracy test

Parameter	Analytical Value	Numerical		
		Mean	Scatter	Error
$u_*$ (m/s)				
Air	1313.4	1316.7	$\pm 0.35\%$	+0.25%
Water	1313.4	1313.5	$\pm 0.02\%$	+0.008%
$p_*$ (MPa)				
Air	2.7495	2.7472	$\pm 0.2\%$	-0.084%
Water	2.7495	2.7900	$\pm 4.3\%$	+1.47%
$T_*$ (K)				
Air	1581.7	1587.3	$\pm 2.0\%$	+0.35%

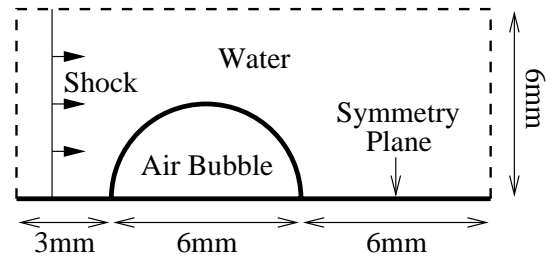


**Fig. 2.** The geometry of the problem

ciated with  $p_*$  in water reflect the extreme sensitivity of the Tait equation of state to small errors in density.

It was concluded that the Vucalm code is capable of simulating the interaction of strong pressure waves with air/water interfaces to a sufficient level of accuracy for the purposes of the present study.

## 5 Problem specification

The problem studied in the present work is illustrated in Fig. 2. As noted in Sect. 1, this problem has been selected to match, as far as is practicable, an experiment reported by Bourne and Field (1992). A cylindrical air cavity, 6 mm in diameter, is immersed in water at ISA sea-level conditions. A 1.9 GPa shock wave (shock Mach number  $\sim 1.9$ ) propagates through the water from left to right; all elapsed times are measured from the first shock/cavity contact. Only the upper half of the problem is simulated; the lower domain boundary represents the plane of symmetry. Boundary conditions on the left boundary are initially fixed at post-shock values (inflow velocity 673 m/s) in order to generate the incoming shock wave, but, from  $t = 0.5 \mu\text{s}$  onwards, non-reflecting boundary conditions are applied in order to allow the escape of left-running waves which are generated by the shock-cavity interaction. The upper and right boundaries are non-reflecting at all times. A mesh of approximately  $5 \times 10^4$  cells has been used; in the initial (unperturbed) mesh, individual cells are square for convenience.

In the original experiment the cylindrical air cavity was cut in a gel block. This was sandwiched between two further gel blocks in order to seal the ends of the cavity, and the whole assembly was immersed in water. An explosive plane wave generator was then used to propagate a shock into the gel assembly normal to the cavity axis. The experiment differed somewhat from the idealised two-dimensional conditions of the simulation in that (i) the shock could interact with the cavity in the third dimension via the sandwiching gel blocks; (ii) the incident shock was somewhat curved; (iii) the pressure behind the shock front decayed rapidly to the (undisclosed) CJ pressure of the explosive. The simulated scenario was considered to be the best practical 2D approximation to the experiment that could be achieved with the available information, but the factors listed above should be remembered when comparing the results of the simulation with experimental data.

## 6 Flow evolution

At the initial conditions, the acoustic impedance of water is approximately 3600 times that of air. Consequently, when the incident water shock strikes the left bubble wall a relatively weak shock is transmitted into the air, and a strong expansion fan is produced in the water, running leftwards and upwards, while the bubble wall is deformed to the right. For the equivalent one-dimensional problem, discussed in Sect. 4, the transmitted shock pressure is 2.75 MPa, giving a shock Mach number  $M_s = 4.8$ , and post-shock temperature  $T_* = 1582$  K. Thus, although the transmitted shock is very weak compared to the incident shock, it is far from negligible in absolute terms, and will produce substantial heating of the bubble gas. In two-dimensions, the spatially non-uniform deformation of the bubble wall yields a higher water velocity on the bubble centreline. This in turn generates additional compression waves in the air which strengthen the air shock – at  $t = 1.2$   $\mu\text{s}$  (Fig. 3) the centreline shock pressure is approximately 4 MPa, falling with distance from the symmetry plane.

After 2.0  $\mu\text{s}$  (Fig. 4) the incident water shock has traversed almost the full cavity width. The interaction between this shock and the expansion waves originating at the bubble surface has resulted in significant weakening and curvature of the shock. The air shock propagates more slowly, and has decoupled from the incident shock, while the left bubble wall has become involuted. The structure of the computational mesh in the vicinity of the cavity at this time is shown in Fig. 5. Note the greatly increased mesh density within the cavity behind the air shock, mirroring the increased air density, and the alignment of mesh cells along the cavity boundary. The latter results from the action of the interface smoothing routine (see Sect. 2).

At  $t = 2.5$   $\mu\text{s}$  (Fig. 6) a distinct water jet has formed running to the right along the symmetry plane. As the jet deforms the left bubble wall, compression waves are produced in the air, which continue to strengthen the air shock. By 2.8  $\mu\text{s}$  (Fig. 7) this shock has formed an oblique reflection at the upper right bubble wall. Figures 8 to 10 show the evolution of the air shock/wall interaction; the

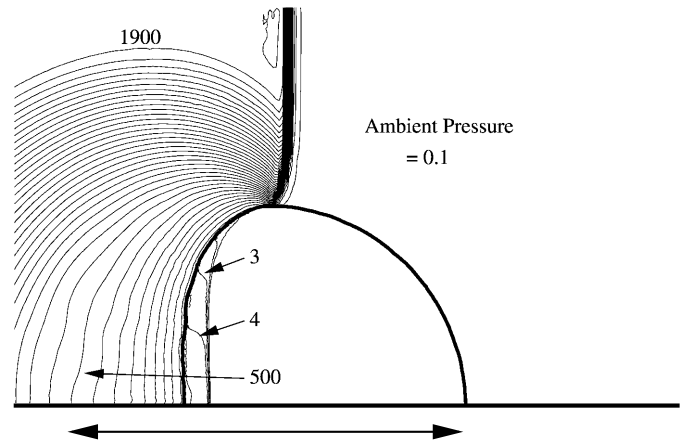


**Fig. 3.** Shock/cavity interaction,  $t = 1.2$   $\mu\text{s}$ . Horizontal arrow indicates initial position and size of bubble; heavy line is bubble wall; contours are pressure:  $\Delta p = 1$  MPa for  $0 < p < 100$  MPa (air only), otherwise  $\Delta p = 50$  MPa; indicated contour values in MPa

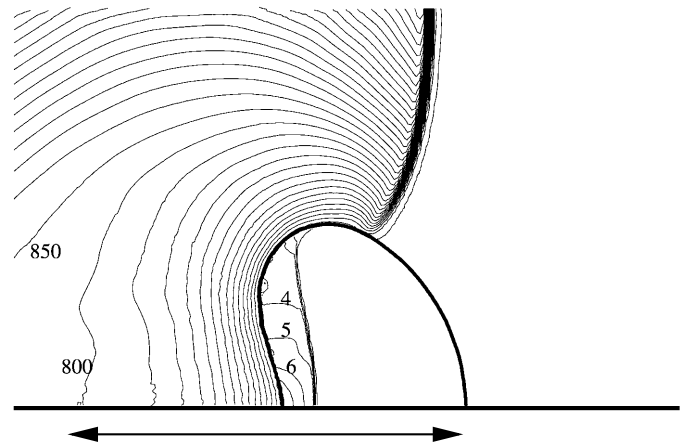


**Fig. 4.** Shock/cavity interaction,  $t = 2.0$   $\mu\text{s}$ . Legend as Fig. 3

incidence angle at the point of reflection increases with time due to the wall curvature, so that after about 40% of the shock length has undergone an oblique reflection, the remainder undergoes a near-normal reflection at around  $t = 2.95$   $\mu\text{s}$ .

At  $t = 3.1$   $\mu\text{s}$  (Fig. 10) the water jet reaches the right bubble wall, cutting the cavity in half. At this stage the peak water velocity in the jet is approximately 2600 m/s. On impact, the jet produces an intense blast wave in the surrounding water with an initial peak overpressure exceeding 4.7 GPa ( $t = 3.2$   $\mu\text{s}$ , Fig. 11). The air cavity resembles a tear-drop, and the air shock, now travelling to the left, has begun to interact with the lower left cavity wall, producing a Mach reflection. At  $t = 3.3$   $\mu\text{s}$  (Fig. 12) the Mach reflection is more apparent. Figure 13 provides a close-up of the velocity and pressure fields in the vicinity of the cavity at this time. Ahead of the airshock (lower left within cavity) typical values for the air temperature, pressure and velocity are approximately 1800 K, 5 MPa, and 2400 m/s, respectively. Behind this shock (upper centre)

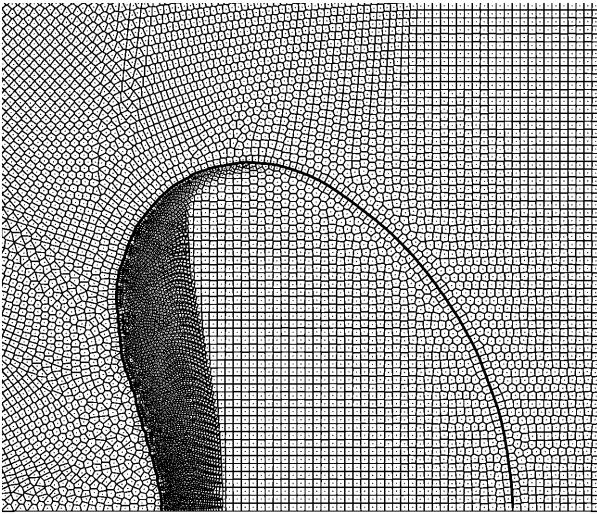


**Fig. 5.** Shock/cavity interaction,  $t = 2.0 \mu\text{s}$ . Close-up of Free-Lagrange mesh. Heavy line is cavity boundary, dots indicate positions of “particles” at which flow properties are stored

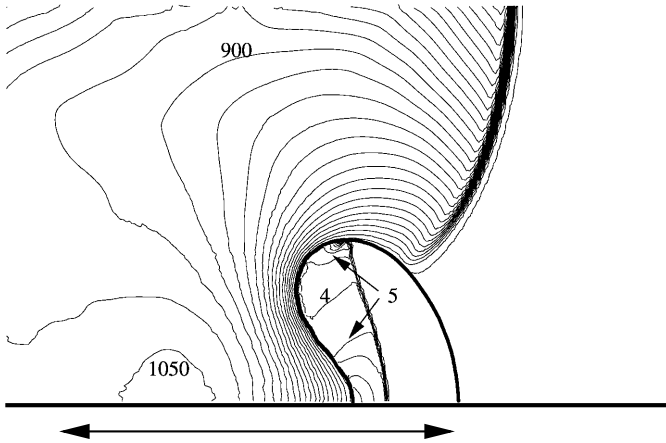


**Fig. 6.** Shock/cavity interaction,  $t = 2.5 \mu\text{s}$ . Legend as Fig. 3. Note water jet at left of bubble

the corresponding values are 5900 K, 35 MPa, and 950 m/s. Finally, after processing by the reflected air shock (lower right) one sees 10800 K, 175 MPa, and 1550 m/s.

The subsequent evolution of the flow is shown in Figs. 14 and 15. The airshock reaches the top of the cavity shortly after  $t = 3.5 \mu\text{s}$ . The shock is curved and converging, so that it strengthens as it propagates. The predicted temperature in the shock-processed air varies with position over the range 5000 K to 12000 K with pressures up to 0.3 GPa. In view of the absence of heat transfer and real gas effects in this simulation, the predicted temperature values should be regarded as only semi-quantitative, but nevertheless indicate that very intense heating of the gas phase does occur. The shape of the developing blast wave is worthy of note; because of the high water velocity in the jet fluid, the wave advances relatively slowly to the left below the bubble, so that the blast front is highly asymmetric. Below and to the right of the cavity, the interaction of

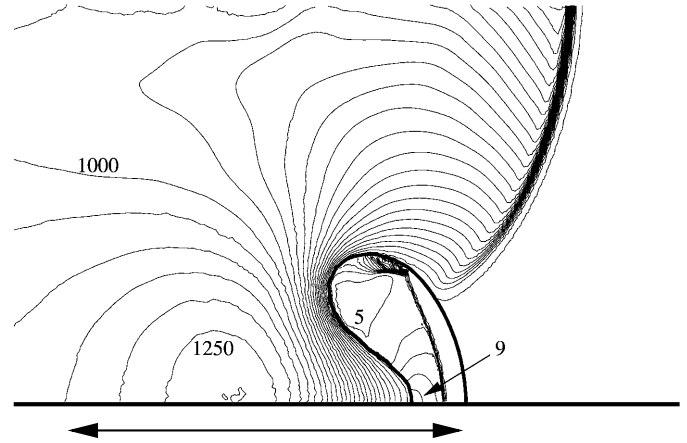


**Fig. 7.** Shock/cavity interaction,  $t = 2.8 \mu\text{s}$ . Legend as Fig. 3. Note oblique reflection of air shock at bubble wall

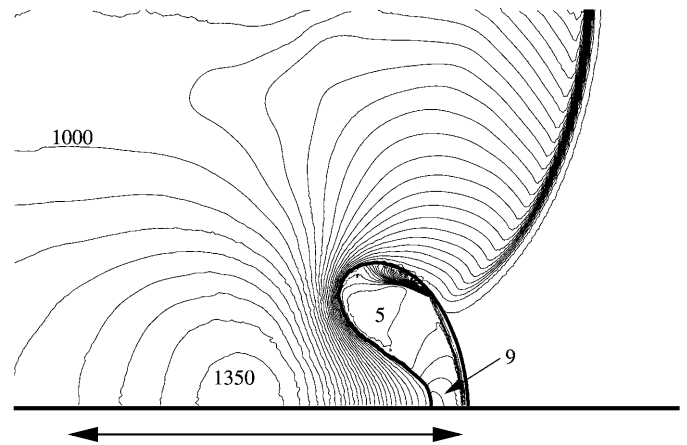


**Fig. 8.** Shock/cavity interaction,  $t = 2.9 \mu\text{s}$ . Legend as Fig. 3

the jet fluid with the surrounding low-momentum water produces a strong counter-clockwise vortex.

The final stage of the simulation is shown in Figs. 16 to 18. At  $t = 3.7 \mu\text{s}$  a further compression wave propagates outwards from the cavity – this appears to result from transmission of the air shock into the water. At the same time, the cavity begins to be drawn into the vortex core due to baroclinicity. The velocity field in the vicinity of the cavity is shown in Fig. 17. By  $t = 3.9 \mu\text{s}$  the cavity has entered the vortex core, where the pressure is  $\sim 1.2$  GPa.

## 7 Discussion and comparison with experiment

The time history of the cavity volume is shown in Fig. 19, normalised by the initial volume,  $V_0$ . The volume reduces linearly with time from  $t \simeq 1.0 \mu\text{s}$  to  $t \simeq 3.1 \mu\text{s}$ , during which interval the volume ratio  $V/V_0$  falls from  $\simeq 0.8$  to  $\simeq 0.1$ . The end of this linear phase correlates closely with the liquid jet impact. Bourne and Field (1992) presented linear volume time histories for cavity collapses from a number of experiments in which 3 mm diameter cavities

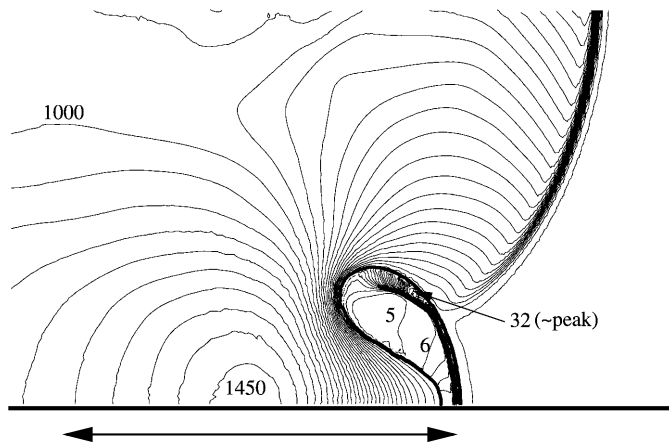


**Fig. 9.** Shock/cavity interaction,  $t = 3.0 \mu\text{s}$ . Legend as Fig. 3. Lower part of air shock has undergone near-normal reflection from right cavity wall (see text)

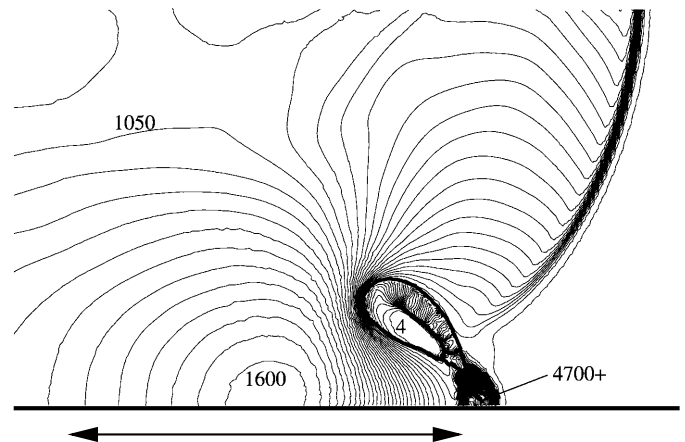


**Fig. 11.** Shock/cavity interaction,  $t = 3.2 \mu\text{s}$ . Legend as Fig. 3. Blast wave is formed; peak overpressure exceeds 4.7 GPa

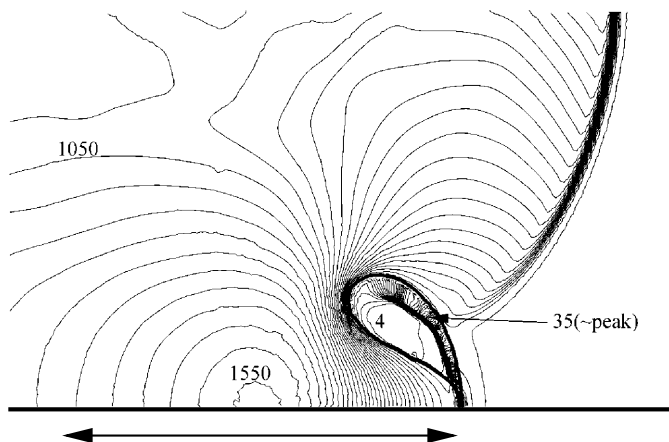


**Fig. 10.** Shock/cavity interaction,  $t = 3.1 \mu\text{s}$ . Legend as Fig. 3. Water jet impacts right bubble wall at approx. 2600 m/s

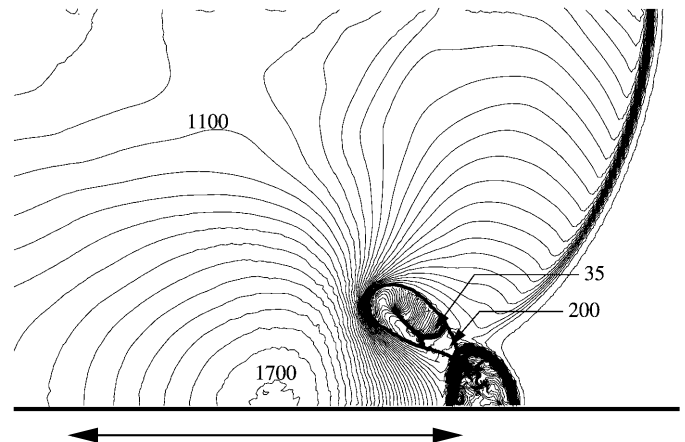


**Fig. 12.** Shock/cavity interaction,  $t = 3.3 \mu\text{s}$ . Legend as Fig. 3. Note Mach reflection of air shock

were impacted by 0.3 GPa shocks. They also reproduced data by Camus (1971) and by Haas and Sturtevant (1987) which show linear histories for other shock-driven collapses of cylindrical cavities. The behaviour of our simulation is therefore in line with previous experimental data in this respect, and adds weight to the idea, voiced by Bourne and Field (1992) that this linear behaviour is a common feature of cylindrical cavity collapses. Following the liquid jet impact, the simulation shows the volume continuing to decline, but at a reduced rate, reaching a minimum at  $t = 3.7 \mu\text{s}$ . At around this time the cavity enters the vortex core and begins to expand under the influence of the reduced local static pressure in the water.

Bourne and Field (1992) observed the collapse of a 6 mm diameter cavity impacted by a 1.9 GPa shock, as simulated in the present work. They present primary data in the form of schlieren photographs of the collapse, taken at  $2 \mu\text{s}$  intervals (their Fig. 5a). The first frame shows the incident shock  $\sim 1.35 \text{ mm}$  from the cavity wall, i.e.  $\sim 0.5 \mu\text{s}$  prior to shock impact. The third frame therefore represents  $t \simeq 3.5 \mu\text{s}$  after shock impact. At this

time the water shock has passed over the cavity, which is hidden from view. However, two small luminous zones are visible, one each side of the symmetry plane. The distance between each zone centre and the symmetry plane is  $\sim 1.1 \text{ mm}$ , and their centre-line location correlates with the downstream boundary of the undisturbed bubble. The luminosity is presumed to originate from the hot gas in the compressed cavity. Therefore, within the limitations of the time resolution of the experimental data, it appears that collapse occurs over a period of  $\sim 3.5 \mu\text{s}$ , and that, at the end of the collapse, the (split) cavity is located close to the undisturbed cavity's downstream boundary, centred at  $\sim \pm 1.1 \text{ mm}$  from the plane of symmetry. Moreover, since two well-separated luminous zones are seen, it is clear that the liquid jet impact must have occurred prior to  $t = 3.5 \mu\text{s}$ .

In the simulated collapse, jet impact occurs at  $t \simeq 3.1 \mu\text{s}$ . At  $t = 3.5 \mu\text{s}$ , the cavity is just upstream of the undisturbed bubble boundary, and  $\sim 1.25 \text{ mm}$  from the plane of symmetry. By  $t = 3.9 \mu\text{s}$  it has closed to  $\sim 1 \text{ mm}$  from the plane of symmetry, and has moved to the undisturbed boundary position. Minimum cavity volume occurs

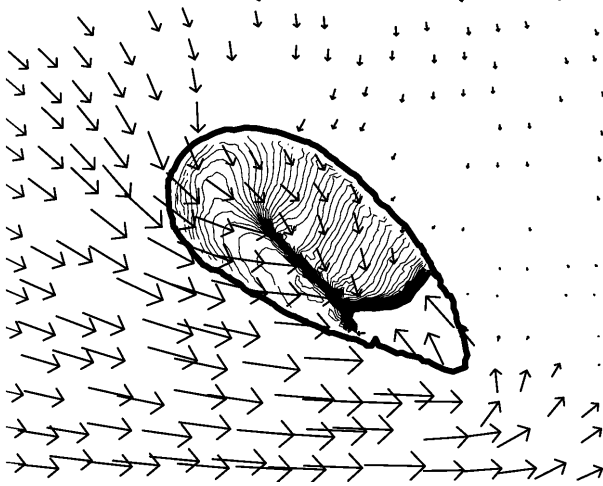


**Fig. 13.** Shock/cavity interaction,  $t = 3.3 \mu\text{s}$ . Close-up of velocity field with vectors for approximately 10% of packets. Pressure contours are shown only within the cavity:  $\Delta p = 1 \text{ MPa}$  for  $0 < p < 100 \text{ MPa}$ . For local gas conditions see text

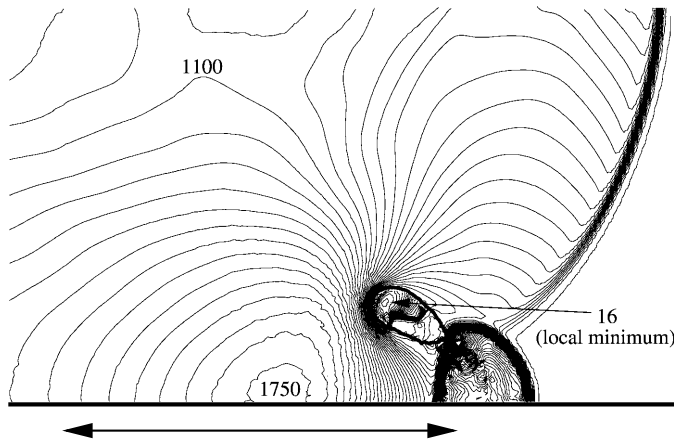


**Fig. 14.** Shock/cavity interaction,  $t = 3.4 \mu\text{s}$ . Legend as Fig. 3

at  $t = 3.7 \mu\text{s}$ . Hence the agreement between simulation and experiment, in terms of the timescales of the collapse and the ultimate location of the compressed cavity, appears to be well within the experimental uncertainty.

In order to obtain a physically meaningful simulation of compressive heating, it is important that mass conservation is obeyed. As discussed in Sect. 2 use of the Free-Lagrange method guarantees exact mass conservation because each computational cell represents a fixed mass of fluid of a single type, and because mass exchange between cells is forbidden. The only exception to the latter rule is that cells of the same type can be combined during “derefinement”, which is nevertheless strictly conservative. However, at the moment of jet impact, approximately 7% of the total cavity mass becomes trapped between the nose of the jet and the far cavity wall, and is retained in the simulation as tiny isolated islands of gas, separate from the main cavity (and not shown on subsequent contour plots). This is probably a numerical artefact, although it is possible (but very difficult to verify experimentally) that such

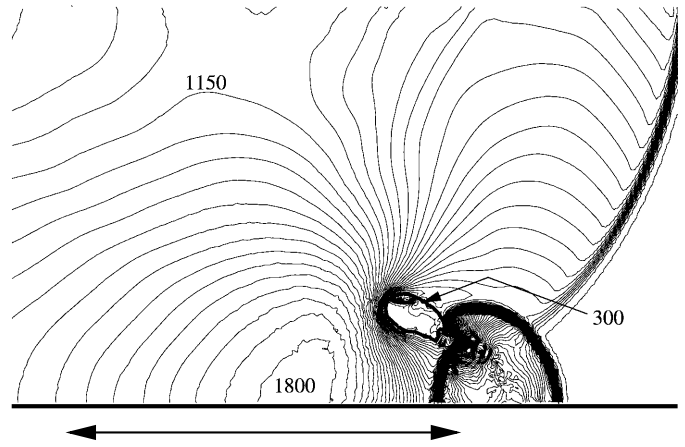


**Fig. 15.** Shock/cavity interaction,  $t = 3.5 \mu\text{s}$ . Legend as Fig. 3. Air shock reaches top of cavity; peak air temperature approx. 12000 K

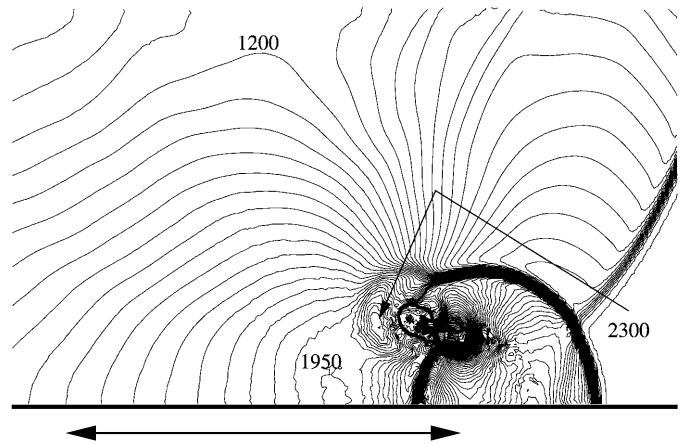


**Fig. 16.** Shock/cavity interaction,  $t = 3.7 \mu\text{s}$ . Legend as Fig. 3. Compression wave propagates from the cavity, which is baroclinically driven towards the vortex core

a mechanism could occur in reality. This isolated mass is included within the volume time history (Fig. 19). It does not represent a conservation error, and will not impact directly on the thermodynamic history of the main cavity, although it will reduce its total volume somewhat.

The mechanism by which compressive heating of the cavity gas occurs, and the degree of applicability of conventional adiabatic models for this process, are of considerable interest. As discussed in Sect. 3, the error in predicted air temperature is expected to become large during the later stages of the cavity compression. Hence the present discussion will be limited to the period up until the liquid jet impact at  $t = 3.1 \mu\text{s}$ , a period which includes the linear compression phase described above. At jet impact, the volume ratio is  $V/V_0 = 0.09$ . If the compression is modelled as spatially uniform and isentropic, the temperature ratio is given by

$$\frac{T}{T_0} = \left(\frac{V}{V_0}\right)^{1-\gamma} \quad (3)$$

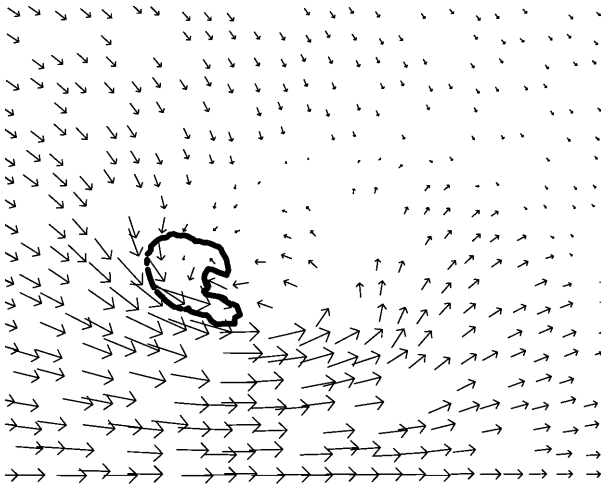


**Fig. 17.** Shock/cavity interaction,  $t = 3.7 \mu\text{s}$ . Close-up of velocity field with vectors for approximately 10% of packets. Note the strong vortical flow centred to the right of the cavity. Water velocity directly below the cavity is  $\sim 2700 \text{ m/s}$

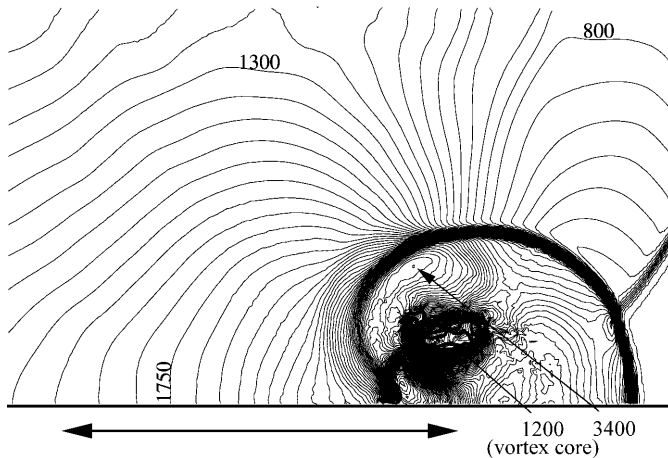


**Fig. 18.** Shock/cavity interaction,  $t = 3.9 \mu\text{s}$ . Legend as Fig. 3. Air cavity has entered in vortex core

Taking  $\gamma = 1.4$  and  $T_0 = 288 \text{ K}$  yields  $T \simeq 755 \text{ K}$ , which corresponds to a pressure of  $2.95 \text{ MPa}$ . The pressure field within the cavity at this time is shown in Fig. 10. The pressure (and temperature) fields display strong spatial variation, due primarily to the presence of a shockwave which is propagating downwards and to the left. Ahead of the shock, typical temperatures and pressures are approximately  $1800 \text{ K}$  and  $4 \text{ MPa}$ , while behind the shock they rise to  $5900 \text{ K}$  and  $35 \text{ MPa}$ . Thus, conditions in the cavity are much more extreme than those predicted using the isentropic model. The time history of the collapse, presented in Sect. 6, shows that shocks are present within the cavity throughout the compression. Moreover, these shocks are of substantial amplitude; the one dimensional analysis of Sect. 4 indicated that the initial air shock would have a shock Mach number of at least 4.8, and this shock is strengthened by subsequent 2D effects and by shock reflection. Thus, we conclude that, for this flow, models based on spatially uniform adiabatic compression are inappropriate;

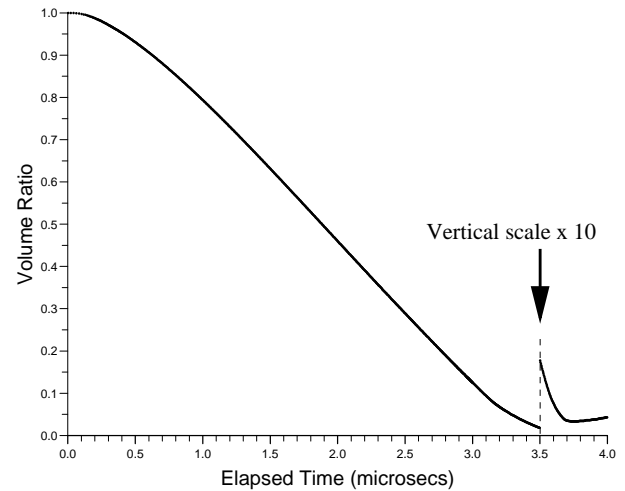


**Fig. 19.** Time history of the cavity volume ratio  $V/V_0$

ate; the compression is fundamentally non-isentropic and spatially non-uniform in character, and is characterised by shock heating. Clearly the errors incurred in assuming isentropic compression will be smaller where the incident shock is weaker – establishing the upper limit of usefulness of such models would be a useful topic for future investigation.

## 8 Conclusions

A Free-Lagrange code has been used to simulate the interaction between a strong underwater shock wave and a cylindrical air cavity. The use of this methodology allows the cavity boundary to be sharply resolved at all times, and ensures exact conservation of mass. The simulation agrees with previously published experimental data in that the volumetric compression is predominantly linear in time, the collapse timescale is correct to within experimental error, and the predicted location of hot gas at the end of the collapse correlates with experimentally observed sources of luminescence. In addition, the simulation predicts many details of the shock/cavity interaction which have not been determined experimentally owing to the extreme practical difficulty of making measurements in this class of flow. The interaction is shown to be physically complex. Gas within the cavity is heated and compressed by a sequence of multiply-reflected shock waves, attaining a final temperature of the order of  $12000+ \text{ K}$ . The conventional assumption of spatially-uniform isentropic compression is shown to be inappropriate in this case, and to grossly underestimate the pressure and temperature attained during compression.

*Acknowledgements.* The authors are grateful to Prof. R. Hillier for advice on the use of the Tait equation, and to Dr. G.T. Roberts for advice on real gas behaviour.

## References

- American Institute Of Ultrasound In Medicine/National Electrical Manufacturers Association (1992) Standard for real-time display of thermal and mechanical indices on diagnostic ultrasound equipment. Publisher AIUM/NEMA
- Apfel RE, Holland CK (1991) Gauging the likelihood of cavitation from short-pulse, low-duty cycle diagnostic ultrasound. *Ultrasound Med Biol* 17:179–185
- Ball GJ (1996) A Free-Lagrange method for unsteady compressible flow: simulation of a confined cylindrical blast wave. *Shock Waves* 5:311–325
- Ball GJ, East RA (1996) Refraction of a blast wave propagating parallel to a contact discontinuity: a Free-Lagrange numerical simulation. *Proceedings of the 20th International Symposium on Shock Waves*, pp 557–562
- Ball GJ, East RA (1999) Shock and blast attenuation by aqueous foam barriers: influences of barrier geometry. *Shock Waves* 9:37–47
- Benjamin TB, Ellis AT (1966) The collapse of cavitation bubbles and the pressures thereby produced against solid boundaries. *Phil Trans R Soc Lond A* 260:221–240
- Blake JR, Taib BB, Doherty G (1986) Transient cavities near boundaries. Part 1. Rigid boundary. *J Fluid Mech* 170:479–497
- Blake JR, Gibson DC (1987) Cavitation bubbles near boundaries. *Ann Rev Fluid Mech* 19:99–123
- Bourne NK, Field JE (1991) Bubble collapse and the initiation of explosion. *Proc Roy Soc Lond A* 435:423–435
- Bourne NK, Field JE (1992) Shock-induced collapse of single cavities in liquids. *J Fluid Mech* 244:225–240
- Bowden FP, Yoffe AD (1952) Initiation and growth of explosion in liquids and solids. Reprinted by Cambridge University Press, 1985
- Bowden FP, Yoffe AD (1958) Fast reaction in solids. London, Butterworths
- Brunton JH, Camus J-J (1970) The application of high-speed photography to analysis of flow in cavitation and drop-impact studies. In: *Proc Int Conf High-speed Photography*. New York, SMPTE, pp. 444–449
- Camus J-J (1971) High-speed flow in impact and its effect on solid surfaces. PhD thesis, University of Cambridge
- Chaudhri MM, Field JE (1974) The role of rapidly compressed gas pockets in the initiation of condensed explosives. *Proc Roy Soc Lond A* 340:113–128
- Chaudhri MM, Almgren A-A, Persson A (1982) High speed photography of the interaction of shocks with voids in condensed media. SPIE vol. 348, 15th Int Cong on High-speed Photography and Photonics, San Diego, pp 388–394
- Chaudhri MM (1989) The initiation of fast decomposition in solid explosives by fracture, plastic flow, friction and collapsing voids. *Proc Ninth Symposium (Intl) on Detonation*, Portland, Oregon, pp 857–868
- Church CC (1989) A theoretical study of cavitation generated by an extracorporeal shock wave lithotripter. *J Acoust Soc Am* 86:215–227
- Coley GD, Field JE (1973) The role of cavities in the initiation and growth of explosion in liquids. *Proc Roy Soc Lond A* 335:67–86
- Dear JP, Field JE (1988) A study of the collapse of arrays of cavities. *J Fluid Mech* 190:409–424
- Dear JP, Field JE, Walton AJ (1988) Gas compression and jet formation in cavities collapsed by a shock wave. *Nature* 332:505–508
- Ebeling KJ (1978) Zum Verhalten kugelförmiger, lasererzeugter Kavitationsblasen in Wasser. *Acustica* 40:229–239
- Field JE (1987) Liquid impact and cavitation erosion processes. In: *Tribology in Particulate Technology*. Adam Hilger, Bristol
- Field JE, Swallowe GM, Heavens SN (1982) Ignition mechanisms of explosives during mechanical deformation. *Proc Roy Soc Lond A* 383:231–244.
- Flores J, Holt M (1981) Glimm's method applied to underwater explosions. *J Comp Phys* 44:377–387
- Frey RB (1985) Cavity collapse in energetic materials. *Proc Eighth Symposium (Intl) on Detonation*, pp 68–80
- Haas J-F, Sturtevant B (1987) Interaction of weak shock waves with cylindrical and spherical inhomogeneities. *J Fluid Mech* 181:41–66
- Heavens SN, Field JE (1974) The ignition of a thin layer of explosive by impact. *Proc Roy Soc Lond A* 338:77–93
- Hinsch K, Brinkmeyer E (1976) Investigation of very short cavitation shock waves by coherent optical methods. *High Speed Photography*, SPIE 97:166–171
- Holland CK, Apfel RE (1989) An improved theory for the prediction of microcavitation thresholds. *IEEE Trans Ultrason Ferroelectr Freq Control* 36:204–208
- Howell BP, Ball GJ (2000) Damping of mesh-induced errors in Free-Lagrange simulations of Richtmyer-Meshkov instability. *Shock Waves*, in press
- Iwai Y, Okada T (1989) A study of cavitation bubble collapse pressures and erosion. Part 2. Estimation of erosion from the distribution of bubble collapse pressures. *Wear* 169:535–564
- Johansson CH (1958) The initiation of liquid explosives by shock and the importance of liquid break up. *Proc Roy Soc Lond A* 246:160–167
- Jones IR, Edwards DH (1960) An experimental study on the forces generated by the collapse of transient cavities in water. *J Fluid Mech* 7:596–609
- Kornfeld M, Suvorov L (1944) On the destructive action of cavitation. *J Appl Phys* 15:495–506
- Lauterborn W, Bolle H (1975) Experimental investigations of cavitation-bubble collapse in the neighbourhood of a solid boundary. *J Fluid Mech* 72:391–399
- Lesser M, Finnström M (1987) On the mechanics of a gas-filled collapsing cavity in a liquid. *Proc 7th Int Conf on Erosion by Liquid and Solid Impact*. Cambridge, UK, paper 23
- Lush PA, Sanada N, Tahayama K (1987) *Proc 7th Int Conf on Erosion by Liquid and Solid Impact*. Cambridge, UK, paper 24
- Mader CL, Taylor RW, Venable D, Travis JR (1967) Theoretical and experimental two-dimensional interactions of shocks with density discontinuities. Los Alamos National Laboratory Report LA-3614
- Mader CL, Kershner JD (1985) The three-dimensional hydrodynamic hot-spot model. In: *Proc Eighth Symposium (Intl) on Detonation*, pp 42–52
- Mader CL, Kershner JD (1989) The heterogeneous explosive reaction zone. In: *Proc Ninth Symposium (Intl) on Detonation*, pp 693–700

- Naudé CF, Ellis AT (1961) On the mechanism of cavitation damage by nonhemispherical cavities collapsing in contact with a solid boundary. *Trans ASME D, J Basic Engng* 83:648–656
- Okada T, Iwai Y (1989) A study of cavitation bubble collapse pressures and erosion. Part 1. A method for measurement of collapse pressures. *Wear* 133:219–232.
- Philipp A, Lauterborn W (1998) Cavitation erosion by single laser-produced bubbles. *J Fluid Mech* 361:75–116
- Preece CM (ed) (1979) *Treatise on Materials Science and Technology*. In: *Erosion* vol 16. New York, Academic
- Preece CM, Hansson I (1981) *Adv in Mech and Phys of Surfaces*. Harwood Acad Pub 1:199–254
- Quirk JJ, Karni S (1994) On the dynamics of a shock-bubble interaction. ICASE Report No.94-75
- Radek U (1972) Kavitationserzeugte Druckpulse und Materialzerstrung. *Acustica* 26:270–283
- Starkenbergh J (1981) Ignition of solid high explosive by the rapid compression of an adjacent gas layer. *Proc 7th Symposium (Intl) on Detonation*, pp 3–16
- Steinberg D (1993) A brief review on cavitation bubble collapse near a rigid boundary. *J Stone Dis* 5:49–59
- Takayama K (1999) Application of Shock Wave Research to Medicine. *Proceedings of the 22nd International Symposium on Shock Waves*, pp 23–32
- Tomita Y, Shima A (1986) Mechanisms of impulsive pressure generation and damage pit formation by bubble collapse. *J Fluid Mech* 169:535–564
- Toro EF, Spruce M, Speares W (1994) Restoration of the contact surface in the HLL Riemann solver. *Shock Waves* 4:25–34
- Toro EF (1997) *Riemann solvers and numerical methods for fluid dynamics: a practical introduction*. Springer, Berlin Heidelberg New York
- Van Leer B (1979) Towards the ultimate conservative difference scheme. V. A second-order sequel to Godunov's method. *J Comp Phys* 32:101–136
- Vogel A, Lauterborn W, Timm R (1989) Optical and acoustic investigations of the dynamics of laser-produced cavitation bubbles near a solid boundary. *J Fluid Mech* 206:299–338
- Walters JK, Davidson JF (1962) The initial motion of a gas bubble formed in an inviscid liquid. Part 1. The two-dimensional bubble. *J Fluid Mech* 12:408–416
- Walters JK, Davidson JF (1963) The initial motion of a gas bubble formed in an inviscid liquid. Part 2. The three-dimensional bubble and the toroidal bubble. *J Fluid Mech* 17:321–336
- Winter RE, Field JE (1975) The role of localised plastic flow in the impact initiation of explosives. *Proc Roy Soc Lond A* 343:399–413
- Zequiri B, Hodnett M, Leighton TG (1997) A strategy for the development and standardisation of measurement methods for high power/cavitating ultrasonic fields – Final project report. NPL Report CIRA(EXT)016